Available online at www.sciencedirect.com
SCIENCE DIRECT®
Journal of Sound and Vibration 272 (2004) 187–206
JOURNAL OF SOUND AND VIBRATION
www.elsevier.com/locate/jsvi

Dynamic analysis of large displacement cable motion with experimental verification

C.G. Koh*, Y. Rong

Department of Civil Engineering, National University of Singapore, Block E1A, #07-03, 1 Engineering Drive 2, Singapore 117576, Singapore

Received 6 November 2002; accepted 20 March 2003

Abstract

Cables used in engineering applications may undergo large displacement motion when subjected to dynamic loads, particularly for cables with relatively low tension. As cables are much weaker in the out-of-plane motion than the in-plane motion, three-dimensional dynamic analysis is often necessary even when the excitation contains only a small out-of-plane component. This paper presents the dynamic analysis of three-dimensional cable motion, accounting for axial, flexural and torsional deformations as well as geometric non-linearity due to large displacements and rotations. The comprehensive study covers analytical formulation, numerical strategy based on an iterative finite difference scheme, and experimental verification by means of shaking table tests. A specific problem of cable motion due to support excitation is used to illustrate the asymmetry and sensitivity of the dynamic tension response associated with geometric non-linearity of large displacement cable motion. The shaking table tests validate the accuracy of the numerical results obtained for both two-dimensional and three-dimensional cases.

1. Introduction

Widely used in many engineering applications, cables often serve as load bearing elements and supports for cable suspended systems and other structural applications such as guyed masts and towers. Cables are typically load adaptive and thus behave non-linear geometrically in general. Typically made of elastomeric material and circular cross-section, cables experience relatively high tension, for instance, in cable-stayed and suspension bridges. If the sag ratio is small, the equilibrium shape can be approximated by a parabola and simplified analysis by linear theory can

*Corresponding author. Tel.: +65-6874-2163; fax: +65-6779-1635.
E-mail address: cgkoh@nus.edu.sg (C.G. Koh).

0022-460X/03/$ - see front matter
doi:10.1016/S0022-460X(03)00326-2

be applied due to the relatively small displacement motion. Extensive research has been carried out on static and dynamics analysis of high-tension cables for several decades, see e.g., Refs. [1–7].

Cables can also be used for purposes other than load bearing. For example, they can be used for transmission of power and signal, and in the form of hoses, fluid and solid particles (e.g., cement). The other type of application is to provide a compliant system to restrain motion, such as underwater cables and mooring lines in offshore and marine engineering. For non-load bearing applications, cable tension is relatively low. Under the effects of dynamic excitation, large amplitude motion occurs due to small restoring force. Geometric non-linearity becomes dominant and conventional linear analysis that assumes small displacements is actually not appropriate [8].

From computational point of view, low-tension cables pose a greater challenge than high-tension cables particularly for dynamic analysis. For practical reasons such as study of fatigue under repeated oscillations and control of large displacement motion, this subject has received increasing attention in recent years [9–14]. Flexural stiffness plays an important role in low-tension cable dynamics, without which singularity arises as numerical algorithms may become unstable when the tension approaches zero anywhere along the cable [9]. A very recent study on cable dynamics also shows that ignoring flexural stiffness gives rise to unacceptable errors in predicting high-order natural frequencies [15]. For numerical stability and accuracy reasons, the effects of flexural stiffness are taken into account in the formulation even though bending moment is normally small for cables.

While most research papers reported only numerical studies, Koh et al. [14] developed a modified box scheme suitable for large displacement dynamics of cables with both numerical simulation study and experimental verification. Furthermore, in addition to displacement profile, this reference studied cable tension in details. While it is relatively easy to obtain good numerical results for displacement, the computation of cable dynamic tension is an order higher and requires special care in order to avoid spurious high-frequency modes [14]. The theoretical formulation and the modified box scheme, which were presented in Ref. [14] to give good results for both displacement and tension in two-dimensional (2-D) problems, are extended herein to deal with three-dimensional (3-D) problems. Furthermore, it is desirable to authenticate the numerical scheme by comparing with experimental results. An experimental verification study is thus performed by using a shaking table to produce support excitation to a single-span cable.

2. Theoretical formulation

Fig. 1 shows a differential segment of the cable in the global (X_1, X_2, X_3) co-ordinate system, X_3 being the vertical axis. The tangent line of the cable segment makes an angle θ to the horizontal X_1-X_2 plane, and its projection on the horizontal plane makes an angle α to the X_1 axis. These two angles are chosen as they bear physical meanings particularly with regards to gravity load, instead of an alternative of defining angles with the three axes by directional cosines. θ may be referred to the "vertical" angle as it measures the angle in the vertical (gravity) plane, whereas α is the "horizontal" angle in the horizontal (non-gravity) plane. The position vector is denoted as $\mathbf{r} = (X_1, X_2, X_3)^{\mathrm{T}}$. The cable force and moment vectors are expressed as, respectively, $\mathbf{p} = (p_1, p_2, p_3)^{\mathrm{T}}$ and $\mathbf{m} = (m_1, m_2, m_3)^{\mathrm{T}}$.

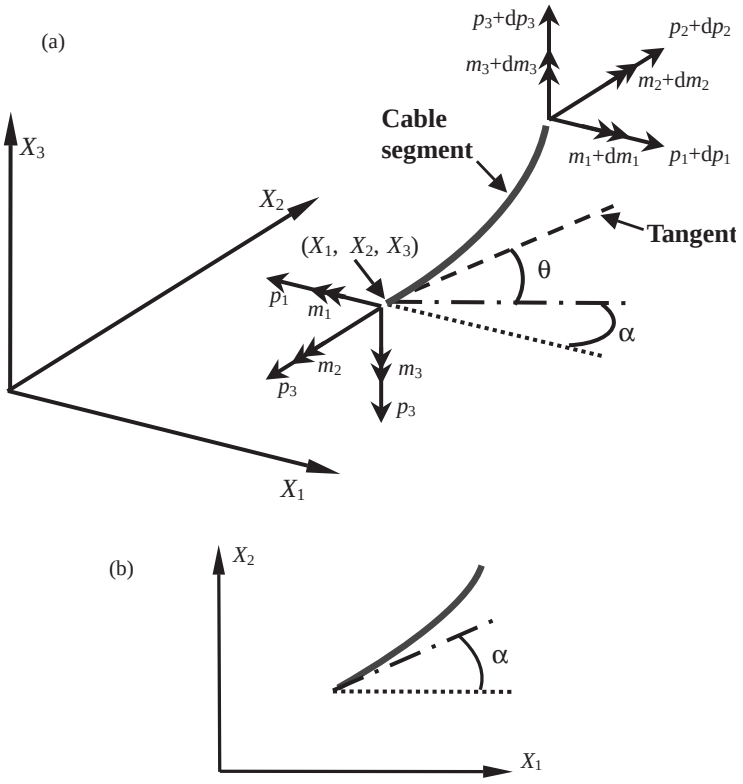

Fig. 1. A differential segment of cable: (a) 3-D illustration; (b) plan view.

The following practical assumptions are made in the formulation:

1. The cable material is homogeneous and isotropic with Young's modulus E, shear modulus G and density ρ.
2. Even though the cable displacement and rotation may be large (mainly due to low flexural stiffness), the strain is small and thus the material constitutive relation remains linearly elastic.
3. Plane section of cable remains plane after deformation.
4. Transverse shear deformation and rotary inertia effects are negligible, whereas axial, flexural and torsional deformations are all included.
5. The cable is circular in cross-section and thus symmetric about the cable axis, with d, A, I and J being the diameter, cross-sectional area, moment of inertia of area and polar moment of inertia of area, respectively.

2.1. Static analysis

The static configuration of cable under the self-weight and given boundary conditions has to be obtained first and used as initial condition for the dynamic analysis. To derive the governing equations, kinematics, equilibrium and constitutive conditions are imposed.

Let ds and ds' be the original and deformed lengths, respectively, of the differential element as shown in Fig. 1. In terms of the angles θ and α defined earlier, the following kinematics relations can be obtained:

$$\frac{dX_1}{ds} = (1+e)\cos\theta\cos\alpha, \tag{1}$$

$$\frac{dX_2}{ds} = (1+e)\cos\theta\sin\alpha, \tag{2}$$

$$\frac{dX_3}{ds} = (1+e)\sin\theta, \tag{3}$$

where e is the axial strain given by

$$e = (ds' - ds)/ds. \tag{4}$$

For equilibrium, the following three equations can readily be written:

$$\frac{dp_i}{ds} = \rho A g \delta_{i3} - f_i(1+e) \quad i = 1,2,3, \tag{5}$$

where f_i denotes the applied force (if any) per unit length in the ith direction. In addition, the self-weight is accounted for in the vertical X_3 direction with g being acceleration due to gravity and δ denoting Kronecker delta function. Moment equilibrium is achieved by

$$d\mathbf{m} - d\mathbf{r} \times \mathbf{p} = \mathbf{0} \tag{6}$$

leading to three equations as follows:

$$\frac{dm_i}{ds} = p_j \frac{dX_k}{ds} - p_k \frac{dX_j}{ds}, \tag{7}$$

where i, j and k take different values of 1, 2 and 3 in permutation.

For constitutive equations, the following two moment-curvature relations can be derived:

$$\frac{d\theta}{ds} = \frac{1}{EI}(m_1 \sin\alpha - m_2 \cos\alpha), \tag{8}$$

$$\frac{d\alpha}{ds} = \frac{1}{EI}(-m_1 \sin\theta\cos\alpha - m_2 \sin\theta\sin\alpha + m_3\cos\theta). \tag{9}$$

When the cable undergoes out-of-plane motion, torsion is induced in general and has to accounted for (unlike in the 2-D case). Torsion can be computed from the three components of $\mathbf{m}$, and its constitutive equation with respect to the twist angle,ϕ, is

$$\frac{d\phi}{ds} = \frac{m_1\cos\theta\cos\alpha + m_2\cos\theta\sin\alpha + m_3\sin\theta}{GJ}. \tag{10}$$

The constitutive equation between the axial force and axial strain is simply

$$e = \frac{T}{EA}, \tag{11}$$

where T is the cable tension and can be obtained from $\mathbf{p}$ as follows:

$$T = p_1 \cos\theta \cos\alpha + p_2 \cos\theta \sin\alpha + p_3 \sin\theta. \tag{12}$$

2.2. Dynamic analysis

For dynamic analysis, it is more convenient to use velocity than displacement as the kinematic unknown. The associated kinematic equations are obtained by differentiating Eqs. (1)–(3) with respect to time, t. Let $v_i = \partial X_i/\partial t$ be the velocity component in the corresponding direction. Accounting for inertia and damping forces, equilibrium Eq. (5) becomes

$$\frac{\partial p_i}{\partial s} = \rho A g \delta_{i3} - f_i(1+e) + \rho A \frac{\partial v_i}{\partial t} + c v_i \quad i = 1, 2, 3. \tag{13}$$

Damping effect is taken into account by adopting equivalent viscous damping with the same damping coefficient, c, in all three directions. Since rotary inertia is neglected, moment equilibrium Eq. (7) is still applicable except that ordinary derivative $\mathrm{d}/\mathrm{d}s$ is now replaced by partial derivative $\partial/\partial s$ since there are two independent variables (s and t). Similarly, the constitutive relations remain the same as in the static analysis given by Eqs. (9)–(11), except for the use of partial derivative $\partial/\partial s$ where appropriate.

Consider a single-span cable of length L. The following dimensionless variables are introduced for convenience:

$$\bar{s} = \frac{s}{L};\quad \bar{X}_i = \frac{X_i}{L};\quad \bar{v}_i = \frac{v_i}{\sqrt{gL}};\quad \bar{t} = \frac{t}{\sqrt{L/g}};\quad \bar{p}_i = \frac{p_i}{EA};\quad \bar{m}_i = \frac{\bar{m}_i L}{EI};$$
$$\bar{f}_i = \frac{f_i L}{EA};\quad \bar{\rho} = \frac{\rho g L}{E};\quad \bar{c} = \frac{cL\sqrt{gL}}{EA};\quad \lambda = \frac{L}{\sqrt{I/A}};\quad \kappa = \frac{EI}{GJ}.$$

There are a total of 12 unknown variables and they can be collected in the following dimensionless vector:

$$\mathbf{u} = \{\, \bar{v}_1 \quad \bar{v}_2 \quad \bar{v}_3 \quad \theta \quad \alpha \quad \phi \quad \bar{p}_1 \quad \bar{p}_2 \quad \bar{p}_3 \quad \bar{m}_1 \quad \bar{m}_2 \quad \bar{m}_3 \,\}^{\mathrm{T}}. \tag{14}$$

The 12 equations required are the three velocity kinematics equations, two moment-curvature relations, one torsion-twist relation and six equilibrium equations as discussed earlier. Where the axial strain (e) appears in these equations, Eqs. (11) and (12) are invoked. The resulting governing equations are non-linear first order partial differential equations in time and space. In view of the fact that the finite difference method will be used in conjunction with an iteration scheme to solve the non-linear equations, it is advantageous to express the 12 governing equations in the following matrix form:

$$\frac{\partial \mathbf{u}}{\partial \bar{s}} = \mathbf{A}\frac{\partial \mathbf{u}}{\partial \bar{t}} + \mathbf{B}, \tag{15}$$

where matrix $\mathbf{A}$ contain mostly zeroes, and the non-zero elements are explained in Appendix A. Vector $\mathbf{B}$ can be split into two vectors as shown in the next section, for numerical efficiency reason.

3. Numerical solution strategy

The governing equations for large displacement cable motion are highly non-linear and coupled. Analytical solution is impossible to obtain and numerical approximation becomes necessary. Among the various numerical methods applied to cable dynamics, the finite difference method and the finite element method are commonly used. The former approximates the differential equations governing the continuum (cable) by a finite number of difference equations, whereas the latter discretizes the continuum physically into a finite number of elements. In practice, each method has its merits and limitations [13,14]. In this paper, the finite difference method is adopted. In particular, the modified box scheme has been shown to give good numerical results for cable displacement and tension for 2-D problems [14]. Though a more general finite difference method, called the generalized-α method, has recently been proposed, there is apparently no clear approach to optimally choosing the parameters required [13].

More importantly, the numerical results obtained by the modified box scheme have been verified by a cable "free fall" experiment involving low tension and large displacement motion [14]. Besides, a detailed investigation of dynamic tension was presented in addition to the usual study of displacement profile. This scheme is thus extended in this study to large displacement cable motion in the 3-D context.

The modified box scheme uses the backward difference method in the time domain and the trapezoidal rule in the space domain. The scheme is implicit and unconditionally stable. Compared with the original box scheme, the modified box scheme has been found to give more stable and more accurate results. Even though the original box scheme is supposedly an order higher in accuracy, it produces results in cable tension containing high-frequency oscillations, the frequency of which increases with decrease in time step [14]. In contrast, the modified box scheme does not have the problem of spurious high-frequency oscillations.

Consider a grid point (i,j) of the modified box scheme at time $\bar{t}_i = i\,\Delta\bar{t}$ and spatial distance $\bar{s}_j = j\,\Delta\bar{s}$, where $\Delta\bar{t}$ is the time step and $\Delta\bar{s}$ the spatial step. Applying the backward difference operator to Eq. (15) in the time domain gives

$$\left(\frac{\partial \mathbf{u}}{\partial \bar{s}}\right)_{i+1} = \mathbf{A}_{i+1}\frac{\mathbf{u}_{i+1} - \mathbf{u}_i}{\Delta\bar{t}} + \mathbf{B}_{i+1}. \tag{16}$$

Use of the trapezoidal rule in the space domain leads to

$$\frac{\mathbf{u}_{i+1,j+1} - \mathbf{u}_{i+1,j}}{\Delta\bar{s}} = \frac{1}{2}(\mathbf{C}_{i,j+1} + \mathbf{C}_{i,j}), \tag{17}$$

where

$$\mathbf{C}_{i,j} = \mathbf{A}_{i+1,j}\frac{\mathbf{u}_{i+1,j} - \mathbf{u}_{i,j}}{\Delta\bar{t}} + \mathbf{B}_{i+1,j}. \tag{18}$$

Eq. (17) can be rewritten as

$$\mathbf{P}_{i,j}\mathbf{u}_{i+1,j+1} + \mathbf{Q}_{i,j}\mathbf{u}_{i+1,j} = \mathbf{R}_{i,j}, \tag{19}$$

where

$$\mathbf{P}_{i,j} = \mathbf{I} - \frac{1}{2}\frac{\Delta\bar{s}}{\Delta\bar{t}}\mathbf{A}_{i+1,j+1}, \tag{20}$$

$$\mathbf{Q}_{i,j} = -\mathbf{I} - \frac{1}{2}\frac{\Delta\bar{s}}{\Delta\bar{t}}\mathbf{A}_{i+1,j}, \tag{21}$$

$$\mathbf{R}_{i,j} = -\frac{1}{2}\frac{\Delta\bar{s}}{\Delta\bar{t}}(\mathbf{A}_{i+1,j+1}\mathbf{u}_{i,j+1} + \mathbf{A}_{i+1,j}\mathbf{u}_{i,j}) + \frac{\Delta\bar{s}}{2}(\mathbf{B}_{i+1,j+1} + \mathbf{B}_{i+1,j}) \tag{22}$$

and $\mathbf{I}$ is an identity matrix. To solve the non-linear equations, Newton–Raphson's method may be adopted which has an advantage of quadratic convergence rate when near the correct solution. This approach has been used in cable dynamic problems; see e.g., Refs. [11,16,17]. A drawback is that it requires the computation and storage of the Jacobian matrix at each time step. If the system size is large, the convergence would be slow especially when the equations are highly non-linear.

Alternatively, an iterative approach can be adopted. To expedite the numerical convergence, vector $\mathbf{B}$ on the right-hand side of Eq. (19) is split into two vectors as follows:

$$\mathbf{B} = \hat{\mathbf{B}}(\mathbf{u}) + \tilde{\mathbf{B}}. \tag{23}$$

The first vector $\hat{\mathbf{B}}$ is a function of unknown variables and can be shifted to the left-hand side of Eq. (19), while the second vector $\tilde{\mathbf{B}}$ remains on the right-hand side. The non-zero elements of these two vectors are given in Appendix A. Good initial guess is generally needed for the iterative approach to work, but this is not a hindrance here since static analysis would provide accurate initial values. This approach has been shown to be computationally faster than using Newton–Raphson method in solving 2-D cable dynamics problems [14].

Substituting Eq. (23) into Eq. (19) and rearranging the terms results in the following matrix equation at a typical grid point:

$$\hat{\mathbf{P}}_{i,j}\mathbf{u}_{i+1,j+1} + \hat{\mathbf{Q}}_{i,j}\mathbf{u}_{i+1,j} = \hat{\mathbf{R}}_{i,j}, \tag{24}$$

where

$$\hat{\mathbf{P}}_{i,j} = \mathbf{I} - \frac{1}{2}\frac{\Delta\bar{s}}{\Delta\bar{t}}\mathbf{A}_{i+1,j+1} - \frac{\Delta\bar{s}}{2}\hat{\mathbf{B}}_{i+1,j+1}, \tag{25}$$

$$\hat{\mathbf{Q}}_{i,j} = -\mathbf{I} - \frac{1}{2}\frac{\Delta\bar{s}}{\Delta\bar{t}}\mathbf{A}_{i+1,j} - \frac{\Delta\bar{s}}{2}\hat{\mathbf{B}}_{i+1,j}, \tag{26}$$

$$\hat{\mathbf{R}}_{i,j} = -\frac{1}{2}\frac{\Delta\bar{s}}{\Delta\bar{t}}(\mathbf{A}_{i+1,j+1}\mathbf{u}_{i,j+1} + \mathbf{A}_{i+1,j}\mathbf{u}_{i,j}) + \frac{\Delta\bar{s}}{2}(\tilde{\mathbf{B}}_{i+1,j+1} + \tilde{\mathbf{B}}_{i+1,j}). \tag{27}$$

Discretizing the cable into n segments and applying Eq. (24) at $j = 0, 1, 2, \ldots, n-1$ for the whole cable yields the following banded matrix equation:

$$\begin{bmatrix} \hat{\mathbf{Q}}_{i,0} & \hat{\mathbf{P}}_{i,0} & 0 & & & \\ 0 & \hat{\mathbf{Q}}_{i,1} & \hat{\mathbf{P}}_{i,1} & 0 & & \\ & & \cdots & & & \\ & & & \cdots & & \\ & & & 0 & \hat{\mathbf{Q}}_{i,n-1} & \hat{\mathbf{P}}_{i,n-1} \end{bmatrix} \begin{bmatrix} \mathbf{u}_{i+1,0} \\ \mathbf{u}_{i+1,1} \\ \cdot \\ \cdot \\ \cdot \\ \mathbf{u}_{i+1,n} \end{bmatrix} = \begin{bmatrix} \hat{\mathbf{R}}_{i,0} \\ \hat{\mathbf{R}}_{i,1} \\ \cdot \\ \cdot \\ \hat{\mathbf{R}}_{i,n-1} \end{bmatrix}. \tag{28}$$

At each time step, the above system contains a total of $12n$ equations and $12(n+1)$ unknowns. Thus, 12 boundary conditions are necessarily imposed to solve the equation system. A flow chart showing the major steps of the numerical procedure is presented in Fig. 2. This study addresses

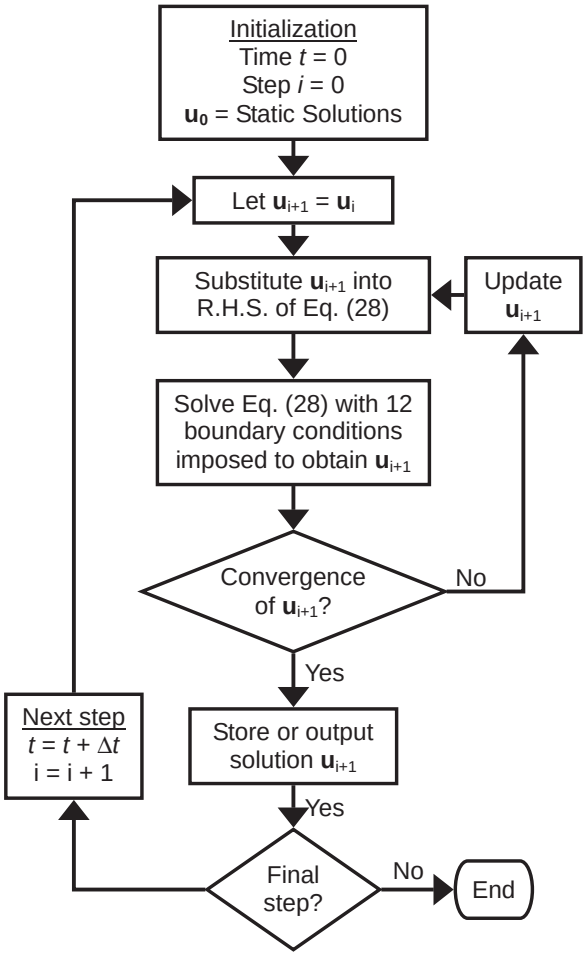

Fig. 2. Flow chart of proposed numerical procedure.

the dynamic response of cable excited by support motion, which is a challenging task. Methods that are used to analyze cables with stationary supports are not necessarily applicable to cables with moving supports [18]. The boundary conditions would clearly depend on the fixity of the two cable ends (e.g., pinned versus fixed end) as well as whether the supports are stationary or moving. Six boundary conditions can be obtained at each end and these will be illustrated in Section 4 for the problem considered.

4. Cable motion due to support excitation

As an example to illustrate the proposed formulation and numerical scheme, a moving support problem is considered. Consider a cable with both ends pinned at the same level. Let D be the horizontal distance between the two ends. The cable is subjected to its self-weight and no other forces. The static solution can readily be obtained and then used as the initial condition for dynamic analysis.

As shown in Fig. 3, the cable plane at the "at-rest" position makes an angle α_0 with the X_1-X_3 plane. Thus, $\alpha = \alpha_0$ along the whole cable before motion begins. One supporting end (A) of the cable is stationary, while the other supporting end (B) undergoes a prescribed motion in the X_1 direction. In the experimental verification study, shaking table is used to provide the support motion and the pin end condition used is illustrated in Fig. 4. At these cross-sections, the bending moments about the local horizontal and vertical axes, viz., m_{xx} and m_{yy} respectively, are zero. It is assumed that the pins physically prevent twist at both ends, but this does not necessarily mean that there is no twist elsewhere along the cable. The corresponding boundary conditions are adopted in the numerical study. Thus, at the stationary end A ($\bar{s} = 0$), the following six boundary conditions are imposed:

$$\bar{v}_1 = \bar{v}_2 = \bar{v}_3 = 0; \quad \phi = 0; \quad \bar{m}_{xx} = 0; \quad \bar{m}_{yy} = 0, \tag{29}$$

where $\bar{m}_{xx}$ and $\bar{m}_{yy}$ are the local bending moments in dimensionless form. They are related to the moments defined in the global co-ordinate system as follows:

$$\bar{m}_{xx} = \bar{m}_2 \cos\alpha - \bar{m}_1 \sin\alpha, \tag{30}$$

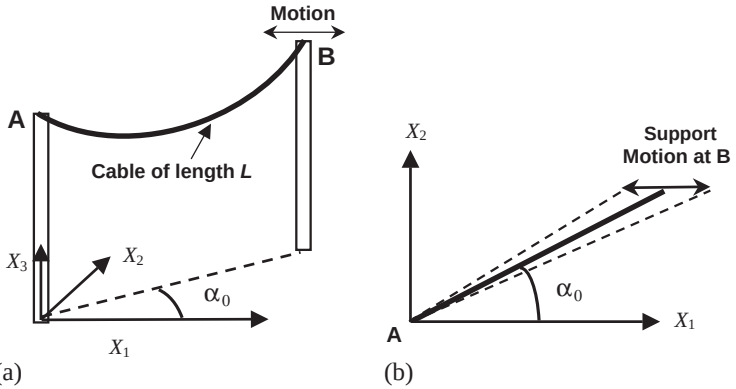

Fig. 3. A single-span cable suspended between two supports: (a) 3-D illustration; (b) plan view.

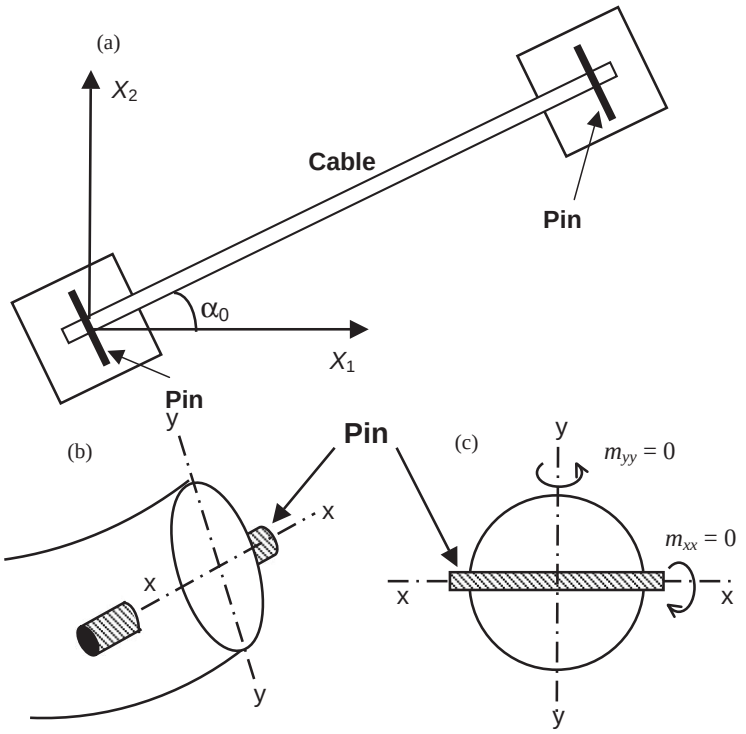

Fig. 4. Pin end boundary conditions: (a) global view of cable; (b) close-up view; (c) cross-sectional view.

Table 1
Displacement and velocity for support motion

Phase	Time, t (s)	Displacement (mm)	Velocity (mm/s)
At rest	0–5	0	0
Rise	5–10	$0.2t'f_1(t')$	$0.2[f_1(t') + tf_2(t')]$
Steady state	10–20	$f_1(t')$	$f_2(t')$
Decay	20–25	$0.2(20-t')f_1(t')$	$0.2[(20-t')f_2(t')-f_1(t')]$

Note: $f_1(t') = 30\sin(2\pi t')$, $f_2(t') = 60\pi\cos(2\pi t')$, and $t' = t - 5$.

$$\bar{m}_{yy} = \bar{m}_1 \sin\theta\cos\alpha + \bar{m}_2 \sin\theta\sin\alpha - \bar{m}_3\cos\theta. \tag{31}$$

The boundary conditions at the moving end B ($\bar{s} = 1$) are similar to end A, except that v_1 is derived from the prescribed support motion. The displacement function for the support motion and the corresponding velocity function are given in Table 1. The support remains at-rest for the first 5 s for warming up of the shaking table in the experiment. Subsequently, there is a rise phase of 5 s before reaching a steady state of sinusoidal motion at 1 Hz and amplitude of 30 mm for 10 s. This is followed by a decay phase of 5 s to zero support motion. The displacement time history of the support motion is shown in Fig. 5.

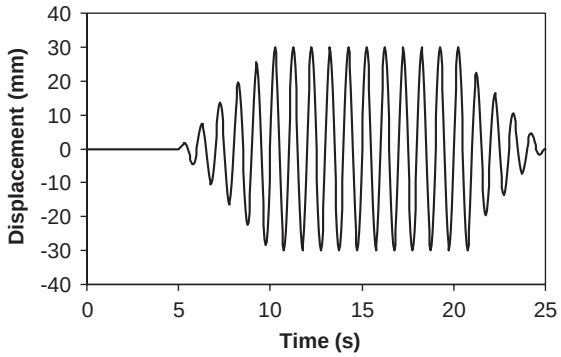

Fig. 5. Displacement time history of support motion.

The dimensions and properties of the rubber cable used are: $L = 1.2\,\text{m}$, $d = 25\,\text{mm}$, $\rho = 1430\,\text{kg/m}^3$, $E = 59\,\text{MPa}$ (determined from a material tensile test in small strain range) and viscous damping ratio $\xi = 6.2\%$ (determined from a cable pull-back test). The damping coefficient (c) is computed from the following formulae [5]:

$$c = 2\xi\sqrt{EA\rho}. \tag{32}$$

4.1. Numerical simulation study

The choice of time step and spatial step will influence the accuracy and efficiency of the numerical scheme. After some convergence study, it is found appropriate to use $\Delta t = 8\,\text{ms}$ and $\Delta s = 30\,\text{mm}$. The latter means that there are 40 segments and 41 nodes (including the two supporting ends) in the numerical model.

4.1.1. Two-dimensional problems

First, numerical simulation study is carried out for 2-D problems, by setting $\alpha_0 = 0$. The horizontal velocity at the mid-span and the dynamic tension (i.e. without the static component) at a distance of 60 mm from the stationary end are studied. Since the support motion is in the same plane containing the initial cable profile, no out-of-plane motion takes place. While keeping the same cable length (L), three values for the at-rest horizontal distance between the two ends are considered: $D = 1.15$, 1.16 and 1.17 m, to study the effect of the sag ratio (i.e., sag/cable length). The corresponding sag ratios are 0.124, 0.111 and 0.0967. The numerical results for the horizontal velocity at the mid-span are presented in Fig. 6. It can be seen that the velocity is not sensitive to small change in the sag ratio and is fairly symmetrical in the positive and negative directions. Nevertheless, the same cannot be said for the tension response. The dynamic tension at 30 mm from the stationary end is presented in Fig. 7. The numerical results show that the dynamic tension increases as the distance between the supports increases. This is because, for a smaller sag ratio, the cable is in a tauter state and any movement would cause a higher change in tension than in the case of larger sag ratio.

Geometric non-linearity is also manifested in the non-proportional increase in the dynamic tension. The increase in the maximum dynamic tension is about two times when the distance

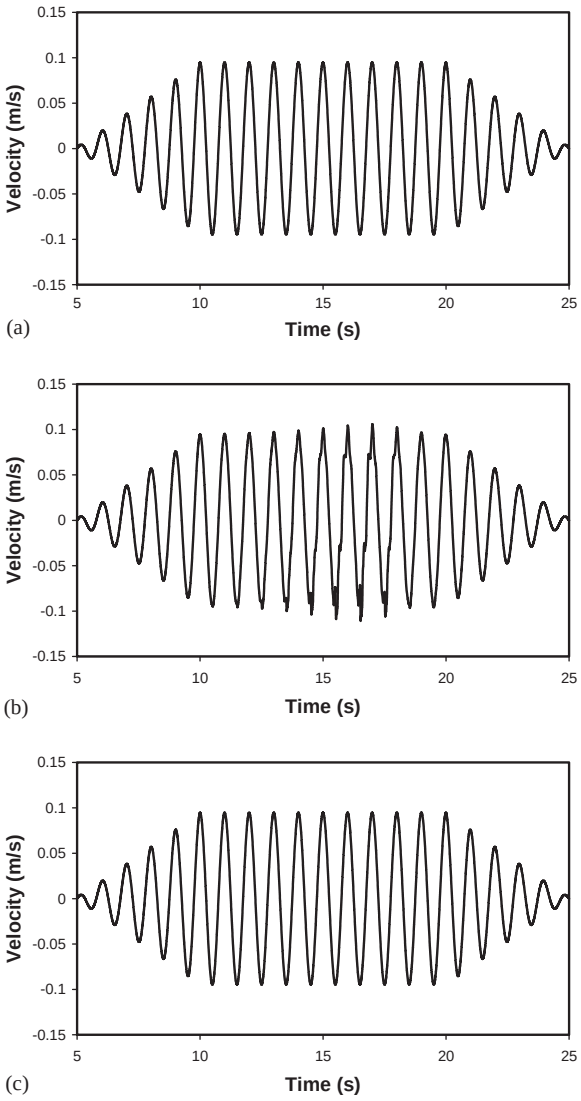

Fig. 6. Horizontal velocity at cable mid-span: (a) $D = 1.15$ m; (b) $D = 1.16$ m; (c) $D = 1.17$ m.

increases by 10 mm from 1.15 to 1.16 m. But the increase is about 10 times when the distance increases by the same amount from 1.16 to 1.17 m. Furthermore, it can be seen that the dynamic tension response is asymmetric about the zero axis that corresponds to the at-rest position (static response). This is not surprising in view of the geometric non-linearity as explained in Fig. 8, where a denotes the amplitude of the imposed support motion. The figure clearly shows that the cable profiles in extreme position 1 (of relatively high sag) and extreme position 2 (low sag) are not symmetric with respect to the at-rest position.

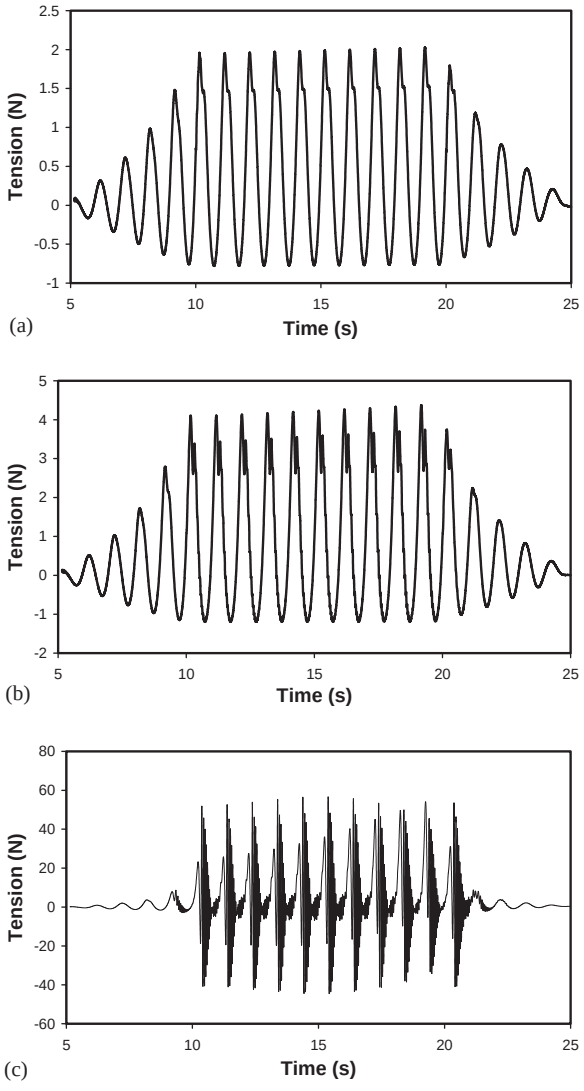

Fig. 7. Cable dynamic tension at 60 mm from the stationary end: (a) $D = 1.15$ m; (b) $D = 1.16$ m; (c) $D = 1.17$ m.

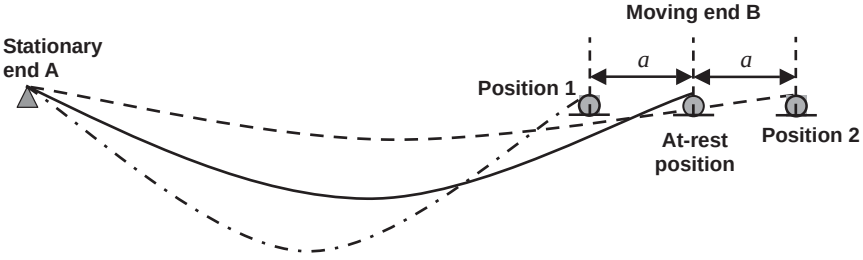

Fig. 8. Schematic sketch of three positions during cable motion.

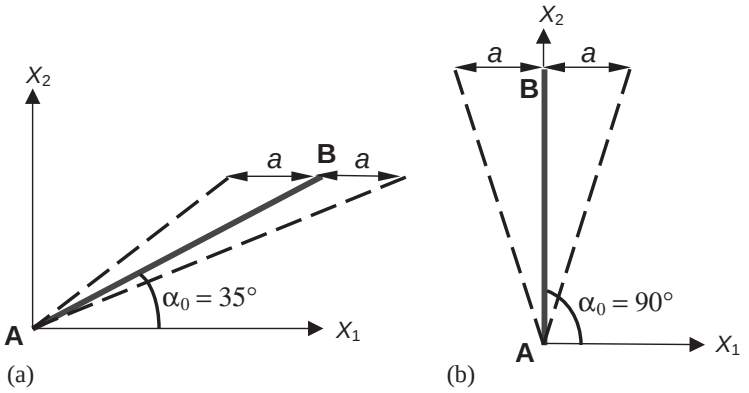

Fig. 9. Plan view of cable support motion: (a) $\alpha_0 = 35^\circ$ and (b) $\alpha_0 = 90^\circ$.

4.1.2. Three-dimensional problems

Next, 3-D dynamic analysis is conducted for several values of α_0. The horizontal distance is fixed at $D = 1.16$ m. Two examples of α_0 at 35° and 90° in plan view are illustrated in Fig. 9. Out-of-plane motion is obviously induced. As an example of velocity presentation, the three components of the cable mid-span velocity are presented in Fig. 10 for the case of $\alpha_0 = 35^\circ$. The velocity is fairly symmetric with respect to zero. This is also true for the displacement response (obtained by numerical integration of velocity) at the mid-span, as presented in Fig. 11. But again the dynamic tension is not so, as will be shown later for both numerical and experimental results (Fig. 15).

The amplitude of support motion is effectively $a\cos\alpha_0$ in the plane of cable and $a\sin\alpha_0$ out of plane as illustrated in Fig. 9. Hence, the larger value of α_0 is, the smaller the in-plane motion is. The converse is true for the out-of-plane motion. Since the tension is mainly due to the in-plane motion, it is expected that the dynamic tension should decrease with an increase in α_0. This is confirmed by the numerical results in Fig. 12 which presents the maximum dynamic tension as a ratio to the 2-D result (at $\alpha_0 = 0$). The trend curve is obtained by fitting a cubic polynomial to the results. The dynamic tension of cable remains relatively unchanged when α_0 is small ($<10^\circ$). Beyond the small angle range, the dynamic tension decreases considerably with increasing α_0.

4.2. Experimental verification study

To validate the numerical model and scheme, an experimental study is performed by means of a shaking table of size 1 m × 1.5 m. As illustrated in Fig. 13, two steel C-channel columns are used to support the two ends of a single-span cable. One of the columns is bolted to the shaking table and the other to strong floor. The full length of the cable is 1.250 m. But between the two pin supports, the cable length is 1.200 m and the at-rest horizontal distance is 1.160 m. Each end of the cable has a small hole for insertion of a threaded bolt. As shown in Fig. 14(a), two nuts are used to prevent sideway sliding of cable along the bolt (particularly arising from the out-of-plane motion). Lubrication oil is added between the nuts and the cable to minimize friction. The dimensions and properties of the rubber cable used in the experimental study are the same as those used in the numerical study presented earlier.

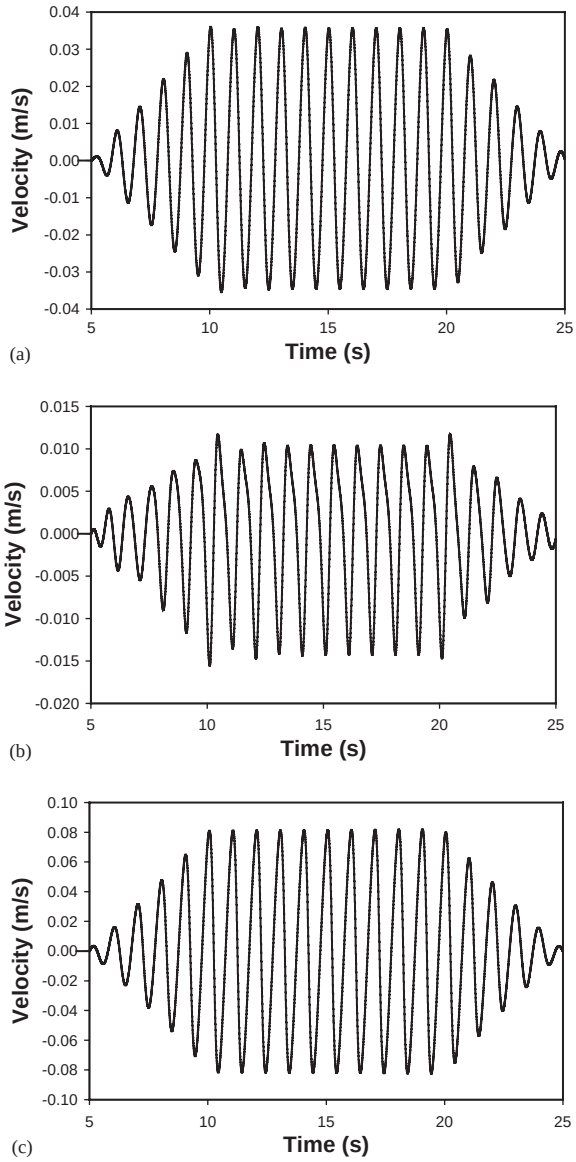

Fig. 10. Velocity component at cable mid-span for $\alpha_0 = 35^\circ$ in the direction of (a) X_1; (b) X_2 and (c) X_3.

The close-up view in Fig. 14(a) also shows some of the strain gauges used to measure the strains. The measurement of strains is at a distance of 60 mm from the stationary end, which corresponds to the third node in the numerical model. This measurement point is chosen near the stationary end in order to minimize the movement effects of electrical wires attached, but not too near the pin hole to avoid stress concentration zone. A total of four strain gauges are attached to the cable in a symmetrical manner, as shown in Fig. 14(b). To measure only the dynamic effect due to support motion, all strain gauges are initialized to zero prior to the activation of the shaking table motion. The signals are transmitted via a dynamic strain meter to a digital

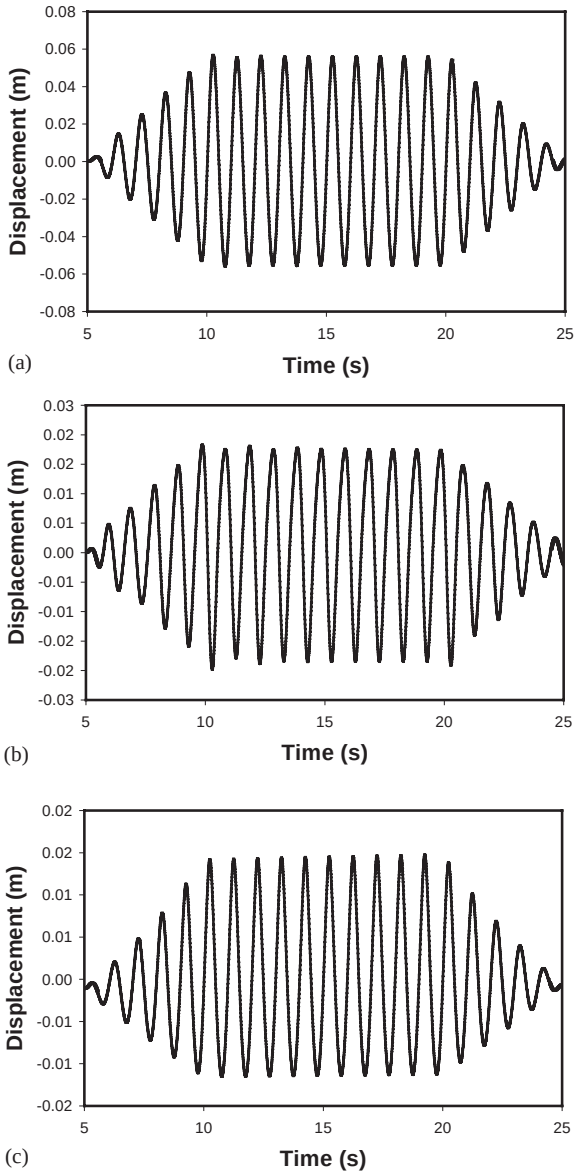

Fig. 11. Displacement component at cable mid-span for $\alpha_0 = 35^{\circ}$ in the direction of (a) X_1; (b) X_2 and (c) X_3.

oscilloscope for display and storage. The average of the four strains is then multiplied by Young's modulus of cable to obtain the dynamic tension.

For the shaking table tests, two horizontal angles are considered: $\alpha_0 = 0$ (2-D) and $\alpha_0 = 35^{\circ}$ (3-D). The latter value for the 3-D case was chosen mainly to satisfy the constraints of limited bolt holes available on the shaking table and strong floor for supporting the columns. The input motion as described earlier (Table 1) is imposed to the shaking table in the direction as shown in Fig. 13. The experimental results for the dynamic tension at the steady state are presented in

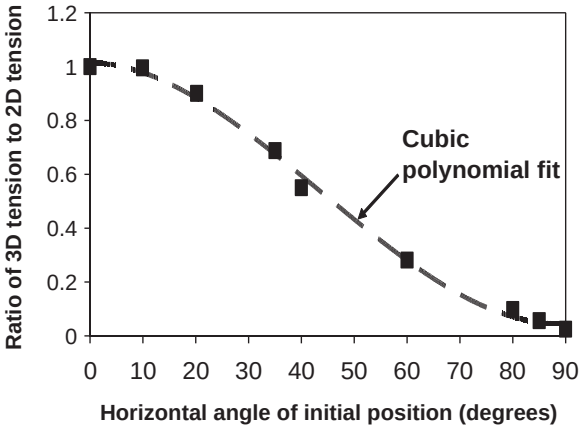

Fig. 12. Numerical result for maximum dynamic tension as ratio to 2-D result.

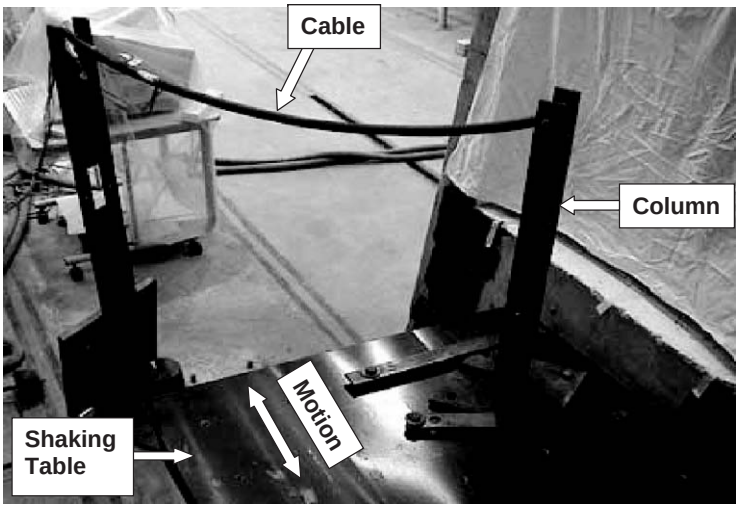

Fig. 13. Experimental set-up of shaking table test for 3-D case ($\alpha_0 = 35°$).

Fig. 15. These results are in good agreement with the numerical results for both the 2-D and 3-D cases, and the errors in terms of the maximum value are less than 10%. The theoretical formulation and numerical scheme presented are hence validated.

5. Conclusions

This paper deals with large displacement cable motion in the 3-D framework. The governing equations are formulated as non-linear first order partial differential equations, taking into account axial, flexural and torsional deformations as well as geometric effects. The modified box scheme, previously developed and verified experimentally (with a cable free-fall problem) for 2-D

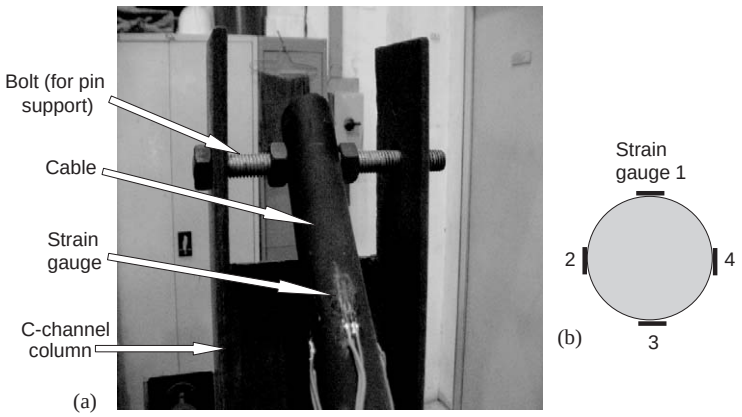

Fig. 14. (a) Close-up view of cable near stationary end support; (b) locations of four strain gauges in cross-sectional view.

cable dynamics, and an iterative procedure for solving the non-linear equations are extended to 3-D cable dynamics problems. A specific problem of cable motion due to support excitation is used to illustrate the numerical scheme and studied experimentally. The following conclusions may be drawn from the research findings presented.

1. The numerical results show that, while the cable velocities do not differ significantly for slightly different sag ratios, the cable dynamic tensions do.
2. In view of the above point and previous finding in Ref. [14] that two different numerical schemes may predict approximately the same cable profile but vastly different results for dynamic tension, it is important to study cable tension (in addition to cable displacement and velocity) in selecting an appropriate numerical scheme.
3. The dynamic tension response is asymmetrical with respect to the static response even when the cable is subjected a symmetrical support motion. The response asymmetry is due to geometric non-linearity associated with varying sag ratios induced by the support motion in the positive and negative directions.
4. The shaking table tests conducted authenticate the accuracy of the numerical results obtained by the modified box scheme for both 2-D and 3-D cases.

Appendix A

A is a matrix of size 12×12 with the following non-zero elements:

$$A_{1,4} = -\sin\theta\cos\alpha - \bar{p}_1 \sin 2\theta \cos^2\alpha - 0.5\,\bar{p}_2 \sin 2\theta \sin 2\alpha + \bar{p}_3 \cos 2\theta \cos\alpha;$$

$$A_{1,5} = -\cos\theta\sin\alpha - \bar{f}_1 \cos^2\theta \sin 2\alpha + \bar{f}_2 \cos^2\theta \cos 2\alpha - 0.5\bar{f}_3 \sin 2\theta \sin\alpha;$$

$$A_{1,7} = \cos^2\theta\cos^2\alpha;\quad A_{1,8} = 0.5\cos^2\theta\sin 2\alpha;\quad A_{1,9} = 0.5\sin 2\theta\cos\alpha;$$

$$A_{2,4} = -\sin\theta\sin\alpha - 0.5\bar{p}_1 \sin 2\theta \sin 2\alpha - \bar{p}_2 \sin 2\theta \sin^2\alpha + \bar{p}_3 \cos 2\theta \sin\alpha;$$

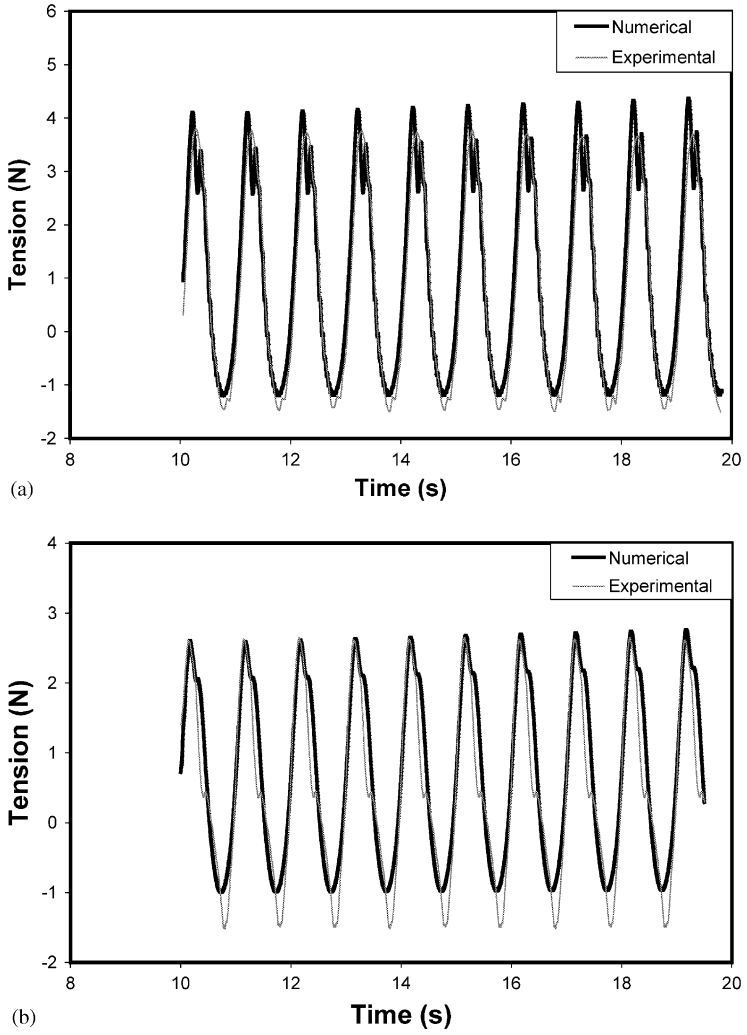

Fig. 15. Cable dynamic tension at steady state: (a) 2-D case ($\alpha_0 = 0$); (b) 3-D case ($\alpha_0 = 30^\circ$).

$$A_{2,5} = \cos\theta\cos\alpha + \bar{p}_1\cos^2\theta\cos 2\alpha + \bar{p}_2\cos^2\theta\sin 2\alpha + 0.5\bar{p}_3\sin 2\theta\cos\alpha;$$

$$A_{2,7} = 0.5\cos^2\theta\sin 2\alpha;\quad A_{2,8} = \cos^2\theta\sin^2\alpha;\quad A_{2,9} = 0.5\sin 2\theta\sin\alpha;$$

$$A_{3,4} = \cos\theta + \bar{p}_1\cos 2\theta\cos\alpha + \bar{p}_2\cos 2\theta\sin\alpha + \bar{p}_3\sin 2\theta;$$

$$A_{3,5} = -0.5\,\bar{p}_1\sin 2\theta\sin\alpha + 0.5\bar{p}_2\sin 2\theta\cos\alpha;\quad A_{3,7} = 0.5\sin 2\theta\cos\alpha;$$

$$A_{3,8} = 0.5\sin 2\theta\sin\alpha;\quad A_{3,9} = \sin^2\theta;\quad A_{7,1} = A_{8,2} = A_{9,3} = \bar{\rho};$$

$\hat{\mathbf{B}}$ and $\tilde{\mathbf{B}}$ are both vectors of size 12 with the following non-zero elements:

$$\hat{B}_4 = m_1\sin\alpha - m_2\cos\alpha;\quad \hat{B}_5 = -m_1\sin\theta\cos\alpha - m_2\sin\theta\sin\alpha + m_3\cos\theta;$$

$$\hat{B}_6 = \kappa(m_1 \cos\theta \cos\alpha + m_2 \cos\theta \sin\alpha + m_3 \sin\theta);\quad \hat{B}_7 = cv_1;\quad \hat{B}_8 = cv_2;\quad \hat{B}_9 = cv_3;$$

$$\hat{B}_{10} = \lambda^2(1+e)(\bar{p}_2 \sin\theta - \bar{p}_3 \cos\theta \sin\alpha);\quad \hat{B}_{11} = \lambda^2(1+e)(-\bar{p}_1 \sin\theta + \bar{p}_3 \cos\theta \cos\alpha);$$

$$\hat{B}_{12} = \lambda^2(1+e)(\bar{p}_1 \cos\theta \sin\alpha - \bar{p}_2 \cos\theta \cos\alpha);$$

$$\tilde{B}_7 = -\bar{f}_1(1+e);\quad \tilde{B}_8 = -\bar{f}_2(1+e);\quad \tilde{B}_9 = \bar{\rho} - \bar{f}_3(1+e)$$

where $e = \bar{p}_1 \cos\theta \cos\alpha + \bar{p}_2 \cos\theta \sin\alpha + \bar{p}_3 \sin\theta$.

References

[1] A. Simpson, On the oscillatory motions of translating elastic cables, *Journal of Sound and Vibration* 20 (1972) 177–189.
[2] C.M. Ablow, S. Schechter, Numerical simulation of undersea cable dynamics, *Ocean Engineering* 10 (1983) 443–457.
[3] N.C. Perkins, C.D. Mote Jr, Three-dimensional vibration of travelling elastic cables, *Journal of Sound and Vibration* 114 (1987) 325–340.
[4] G.V. Rao, R.N. Iyengar, Seismic response of a long span cable, *Earthquake Engineering and Structural Dynamics* 20 (1991) 243–258.
[5] N.B. Kahla, Dynamics of a single guy cable, *Computers and Structures* 54 (1995) 1197–1211.
[6] Y.Q. Ni, W.J. Lou, J.M. Ko, Hybrid pseudo-force/Laplace transform method for non-linear transient response of a suspended cable, *Journal of Sound and Vibration* 238 (2000) 189–214.
[7] H.Y. Hu, D.P. Jin, Non-linear dynamics of a suspended traveling cable subject to transverse fluid excitation, *Journal of Sound and Vibration* 239 (2001) 515–519.
[8] J.W. Leonard, *Tension Structures*, McGraw-Hill, New York, 1988.
[9] A.P. Dowling, The dynamics of towed flexible cylinders: part 1 neutrally buoyant elements, *Journal of Fluid Mechanics* 187 (1988) 507–532.
[10] J.W. Leonard, Nonlinear dynamics of cables with low initial tension, *Journal of Engineering Mechanics ASCE* 98 (1972) 293–309.
[11] C.T. Howell, Numerical analysis of 2-D nonlinear cable equations with applications to low-tension problems, in: *Proceedings of the First International Offshore and Polar Engineering Conference*, Edinburgh, 1991, Vol. 2, pp. 203–209.
[12] M.S. Triantafyllou, C.T. Howell, Nonlinear impulsive motions of low tension cables, *Journal of Engineering Mechanics ASCE* 118 (1992) 807–830.
[13] J.I. Gobat, M.A. Grosenbaugh, M.S. Triantafyllou, Generalized-alpha time integration solutions for hanging chain dynamics, *Journal of Engineering Mechanics ASCE* 128 (2002) 677–687.
[14] C.G. Koh, Y. Zhang, S.T. Quek, Low-tension cable dynamics: numerical and experimental studies, *Journal of Engineering Mechanics ASCE* 125 (1999) 347–354.
[15] Y.Q. Ni, J.M. Ko, G. Zheng, Dynamic analysis of large-diameter sagged cables taking into account flexural rigidity, *Journal of Sound and Vibration* 257 (2002) 301–319.
[16] F. Milinazzo, M. Wilkie, S.A. Latchman, An efficient algorithm for simulating the dynamics of towed cable systems, *Ocean Engineering* 14 (1987) 513–526.
[17] J.J. Burgess, Modelling of undersea cable installation with a finite difference method, in: *Proceedings of the First International Offshore and Polar Engineering Conference*, Edinburgh, 1991, Vol. 2, pp. 222–227.
[18] N.C. Perkins, Dynamic stability of cables subjected to an axial periodic load—Discussion, *Journal of Sound and Vibration* 156 (1992) 361–365.